Scientia Iranica, Vol. 15, No. 1, pp 1 7

SCIENTIA IRANICA

Effect of Alkali-Aggregate Reactions in Concrete Dams Using Finite Element Method

M. Moshtagh[1] and M. Ghaemian[*]

The effect of Alkali-Aggregate Reactions (AAR) in concrete dams was investigated using the finite element method. Two models have been presented to assess the effects of the AAR in concrete dams. The stress dependency of AAR strains has been taken into account in the models and the degradation of concrete properties during the reaction has been implemented in the finite element program. The results of the isothermal and nonisothermal analyses of a gravity section of a Beauharnois power plant have been presented and compared with the measured data and the results are in close agreement. The results of the analysis demonstrate the importance of the AAR in concrete dams. High stresses and large deflections occur in the dam during the reaction. Because of the stress dependency of the reaction, vertical displacements are smaller than horizontal displacements.

INTRODUCTION

The Alkali-Aggregates Reaction is a chemical reaction that occurs between hydroxide ions found in the form of K(OH) and Na(OH) in the Portland cement and reactive aggregates. Water, as a main component of concrete, is a catalyzer in this reaction. AAR causes concrete expansion, micro cracks and, finally, visible cracks in the concrete. Because water is required for continuance of the reaction, in dams, mass concrete, where humidity is at its extreme, the reaction can continue during the age of the structure. Over a long period of time, AAR affects the operation of concrete gravity dams, due to deterioration induced by the AAR. The structural effect of AAR is the resulted strain, due to the expansion of the concrete volume produced by the generation of reaction products, such as Silica gel. This strain is related to temperature, humidity, aggregate activity and stresses on the structure [1]. Concrete properties, such as modulus of elasticity and tensile strength, are degredaded during the reaction.

Few models are proposed by researchers, taking into consideration AAR. A parametric model for AAR was proposed by Leger et al. [2]. They applied a CTMR loop to assess the effects of AAR in concrete dams. Capra and Bournazel [3] introduced a thermodynamic model of damaged concrete, in which temperature, relative humidity, applied stress and aggregate activity are the main factors contributing to AAR. Huang and Pietruszczak [4] applied a nonlinear continuum theory to model the thermo mechanical behavior of concrete subjected to an alkali-silica reaction. The expansion rate was assumed to be controlled by the alkali content and the magnitude of confining stress, as well as temperature variation.

Bournazel et al. [5] prepared a probabilistic model, in which the size of particles, aggregate activity, concentration of reactive aggregates and the probability of Na^+, K^+ and OH existence in the system were taken into consideration.

In this paper, two models have been presented to study AAR effects in concrete dams. In the models, the stress dependency of the strain has been taken into account. Spatial changes of humidity and aggregate activity have been neglected through the dam body [2].

FINITE ELEMENT IMPLEMENTATION

Strain caused by AAR is introduced into a finite element program. This strain is implemented in the form of the initial strain into the system. In a system with initial strain, the stress-strain relationship is as follows:

$$\{\sigma\} = [D](\{\varepsilon\} \quad \{\varepsilon_0\}), \tag{1}$$

1. *Department of Civil Engineering, Sharif University of Technology, P.O. Box 11155-9313, Tehran, I.R. Iran.*

*. *Corresponding Author, Department of Civil Engineering, Sharif University of Technology, P.O. Box 11155-8639, Tehran, I.R. Iran.*

where $\{\sigma\}$ is the stress tensor, ε is the total strain tensor, ε_0 is the initial strain tensor and $[D]$ is the material properties matrix.

The strain energy of an element is as follows:

$$U_e = \frac{1}{2}t\int_{\Omega}\{\{\varepsilon\} \quad \{\varepsilon_0\}\}^T\{\sigma\}d\Omega$$

$$= \frac{1}{2}t\int_{\Omega}\{\{\varepsilon\} \quad \{\varepsilon_0\}\}^T[D]\{\{\varepsilon\} \quad \{\varepsilon_0\}\}d\Omega. \tag{2}$$

The above equation can be modified as the following:

$$U_e = \frac{1}{2}t\int_{\Omega}\{\varepsilon\}^T[D]\{\varepsilon\}d\Omega \quad \frac{1}{2}t\int_{\Omega}\{\varepsilon\}^T[D]\{\varepsilon_0\}d\Omega$$

$$\frac{1}{2}t\int_{\Omega}\{\varepsilon_0\}^T[D]\{\varepsilon\}d\Omega + \frac{1}{2}t\int_{\Omega}\{\varepsilon_0\}^T[D]\{\varepsilon_0\}d\Omega. \tag{3}$$

The second and third terms on the right hand side of the equation are equal. The strain-displacement relationship is as follows:

$$\{\varepsilon\} = [B]\{\delta^e\}, \tag{4}$$

where $\{\delta^e\}$ is the vector of the element degrees of freedom and $[B]$ is the strain-displacement matrix.

By inserting Equation 4 into Equation 3, the strain energy can be rewritten into the following form:

$$U_e = \frac{1}{2}t\{\delta^e\}^T\int_{\Omega}[B]^T[D][B]d\Omega\{\delta^e\}$$

$$+ \frac{1}{2}t\int_{\Omega}\{\varepsilon_0\}^T[D]\{\varepsilon_0\}d\Omega$$

$$t\{\delta^e\}^T\int_{\Omega}[B]^T[D]\{\varepsilon_0\}d\Omega. \tag{5}$$

By making use of the definition of the stiffness matrix, $[K_e] = t\int_{\Omega}[B]^T[D][B]d\Omega$, the above equation can be recast as follows:

$$U_e = \frac{1}{2}\{\delta^e\}^T[K_e]\{\delta^e\} + \frac{1}{2}t\int_{\Omega}\{\varepsilon_0\}^T[D]\{\varepsilon_0\}d\Omega$$

$$t\{\delta^e\}^T\int_{\Omega}[B]^T[D]\{\varepsilon_0\}d\Omega. \tag{6}$$

The second term on the right hand side is constant. The potential energy of an element can be written as follows:

$$\Pi_e = U_e \quad W_e$$

$$= \underbrace{\frac{1}{2}\{\delta^e\}^T[K_e]\delta^e \quad \{\overline{F}_e\}^T\{\delta^e\} + \text{Cons}}_{U_e}$$

$$\underbrace{\{F_e\}^T\{\delta^e\}}_{W_e}, \tag{7}$$

where $\{F_e\}$ is the element load vector and is as follows:

$$\{\overline{F}_e\} = t\int_{\Omega}[B]^T[D]\{\varepsilon_0\}d\Omega.$$

Minimizing the potential energy results in the following:

$$[K_e]\{\delta^e\} = \{F_e\} + \{\overline{F}_e\}. \tag{8}$$

Therefore, the effect of initial strains is implemented in the total load vector of the system.

COMMON ASSUMPTIONS OF THE MODELS

In both proposed models, the effects of temperature and applied stresses have been taken into consideration, using weighed factors (F_σ, F_T). The rate of the strain, due to the reaction is as follows:

$$\dot{\varepsilon}_r = f(\dot{\varepsilon}_u, F_T, F_\sigma, t), \tag{9}$$

where $\dot{\varepsilon}_r$ is restrained expansion rate, $\dot{\varepsilon}_u$ is unrestrained expansion rate, F_T represents variation, with respect to temperature, F_σ represents variation, with respect to stresses and t is time.

To consider the effect of temperature, a hyperbolic relationship was defined for F_T as follows [6]:

$$F_T = f(T) = \frac{1}{2}\left(1 + \tanh\left(\frac{T \quad T_0}{A_2}\right)\right), \tag{10}$$

where A_2 and T_0 are material constants and T is temperature. For low temperatures, the function approaches zero and, for high temperatures, it approaches unity.

An important noticeable fact is that the AAR activity will stop below a certain temperature. In this paper, a temperature of 10°C has been assumed as the boundary temperature [2,7]. So, the effect of temperature will be as follows:

$$\begin{cases} F_T = 0 & \text{if } T < 10^\circ\text{ C} \\ F_T = f(T) & \text{if } T \geq 10^\circ\text{ C} \end{cases}. \tag{11}$$

An effective modulus of elasticity was used to consider the effect of creep in the concrete:

$$E_e = \frac{E}{1+\phi}. \tag{12}$$

In the above equation, E_e is the effective modulus of elasticity and ϕ is the creep coefficient. For simplicity, a constant creep coefficient equal to 1.5 [2] was used.

THERMAL ANALYSES

A thermal analysis was performed to obtain temperature distribution in the dam body. Air temperatures are based on the temperature records that was employed by Leger et al. [8]. Only convection and radiation were considered in the analysis and the effects of supplied heat flux from the sun were neglected. The parameters of the thermal analyses are as follows:

Thermal conductivity = 2.62 N/S°C,
Specific heat capacity = 912 m^2/S^2,
Convective coefficient = 23.2 N/mS°C,
Radiation coefficient = 4.2 N/mS°C,
Free-stress temperature = 5°C,
Thermal expansion coefficient = 1.5×10^{-5}/°C.

To consider the effects of convection and radiation simultaneously, an equivalent convective coefficient of 27.4 N/mS°C was used.

In the isothermal analyses, a constant temperature of 5.46°C was employed to the whole dam body.

In this paper, a monolith of the Beauhrnois power plant gravity dam was analyzed. The selected section and the finite element mesh are shown in Figure 1.

FIRST PROPOSED MODEL

In this model, the influences of the effective parameters on the AAR induced strain are as follows.

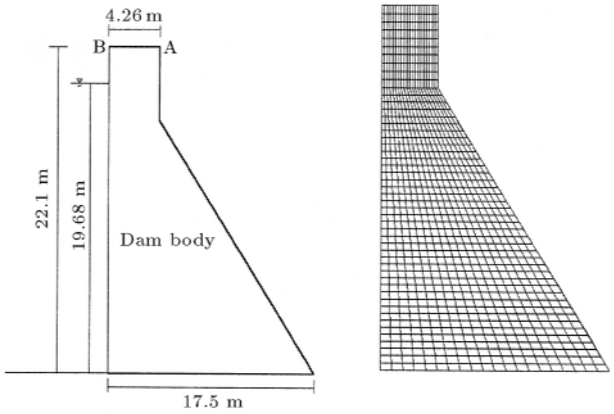

Figure 1. Dam configuration and finite element model.

Effect of Applied Stresses

The exponential function suggested by Hobbs [9] was used to take into account the effect of applied stresses as follows:

$$F_\sigma = f(\sigma) = \exp\left(\frac{A_1\sigma}{f_{c0}}\right), \tag{13}$$

where F_σ is weighed factor of applied stresses, f_{C0} is initial compressive strength, A_1 is material constant and σ is the average of the principal stresses.

In this model, the effect of tension in the AAR strain is neglected, so:

$$\begin{cases} F_\sigma = 1 & \text{if } \sigma \geq 0 \\ F_\sigma = f(\sigma) & \text{if } \sigma < 0 \end{cases} \tag{14}$$

Time Dependency of the Reaction

The time dependency of the reaction has been implemented in this model as follows [10]:

$$f(t) = \frac{\varepsilon\ 1\ \frac{g_3}{\varepsilon})}{A_3}, \tag{15}$$

where:

$$g_3 = \frac{\varepsilon t'}{A_3 + t'}.$$

In the above equation, ε and A_3 are material constants and t' is a fictitious time, called thermal activation time, which shows the progress of the reaction. g_3 represents the free expansion at a given alkali content and is modified during the continuance of the reaction [4]. Because the reaction stops below the boundary temperature, increments of the activation time must be computed at each time step as follows:

$$\begin{cases} dt_{\text{activation}} = 0 & \text{if temperature} < 10°C \\ dt_{\text{activation}} = dt & \text{if temperature} \geq 10°C \end{cases}$$

$$t' = t' + dt_{\text{activation}}. \tag{16}$$

Finally, the rate of the AAR caused strain is:

$$\dot{\varepsilon}_{\text{AAR}} = F_T \times F_\sigma \times f(t). \tag{17}$$

This is added to the initial strains of the system. For nonisothermal conditions, in the elastic range:

$$\dot{\varepsilon}_0 = \underbrace{\frac{1}{3}\dot{\varepsilon}_{\text{AAR}}}_{\text{AAR expansion}} + \underbrace{\frac{1}{3}\alpha\dot{T}}_{\text{Thermal strain}}. \tag{18}$$

In isothermal conditions, the thermal strains are neglected, so the rate of the initial strain is as follows:

$$\dot{\varepsilon}_0 = \frac{1}{3}\dot{\varepsilon}_{\text{AAR}}. \tag{19}$$

Degradation of Concrete Properties

Degradation of the mechanical properties of concrete, particularly the elastic modulus and uniaxial compressive/tensile strength, come mainly from mechanical damage to the material. A simple function, in order to modify the Young's modulus of elasticity and the uniaxial compressive strength during the reaction, was used as follows:

$$E = E_0 \left(1 \quad (1 \quad b_1)\frac{g_3}{\varepsilon}\right), \tag{20}$$

$$f_c = f_{c0} \left(1 \quad (1 \quad b_2)\frac{g_3}{\varepsilon}\right), \tag{21}$$

where E_0 is the initial modulus of elasticity, f_{c0} is the initial compressive strength, g_3 is the free expansion at a given alkali content and b_1 and b_2 are material constants.

Material Parameters

The numerical simulations have been carried out, assuming $E_0 = 15$ MPa and $f_{C0} = 27$ MPa. The constants appearing in $f(T)$ were selected, based on experimental results reported by Pleau et al. [6], i.e. $T_0 = 24.75°C$ and $A_2 = 15.25°C$. The remaining material parameters were chosen as $A_1 = 0.1$, $A_3 = 8200$ days, $\varepsilon = 0.057$, $b_1 = 0.7$ and $b_2 = 0.9$ [4]. The duration of the analysis is 50 years, assuming one month time steps.

Results of the Isothermal Analysis

A finite element analysis of the Beauharnois dam was performed in the isothermal case, where a constant temperature was considered for the dam body.

Figure 2 shows the contours of horizontal and vertical displacements after 25 years of continuing reaction in the isothermal case. Horizontal and vertical displacements of point A are less than measured data, while the vertical computed displacement of point B is greater than the measured one.

Results of the Nonisothermal Analysis

Figure 3 shows the contours of horizontal and vertical displacements after 25 years of continuing reaction in the nonisothermal case. Horizontal displacement of point A has been computed, which is less than the measured data, inversely, the vertical displacement of point B has been found to be greater than the real value.

SECOND PROPOSED MODEL

In this model, effective parameters have been considered as follows.

Stress Dependency of the Strain

A logarithmic function, suggested by Charlwood [1] for the influence of applied stresses, was used. Like the first model, the increasing effect of tension is neglected, so one has:

$$\begin{cases} F_\sigma = 1 & \text{if } \sigma > 0 \\ & \text{if } \sigma \le 0 \Rightarrow \sigma_{abs} = abs(\sigma) \end{cases}$$

$$\Rightarrow \begin{cases} F_\sigma = 1 & \text{if } \sigma_{abs} < \sigma_L \\ F_\sigma = 1 \quad K_1 \log\left(\frac{\sigma_{abs}}{\sigma_L}\right) & \text{if } \sigma_L \le \sigma_{abs} \le \sigma_{\max} \end{cases} \tag{22}$$

where σ_L is compressive stress, below which restrained growth rate is equal to the free expansion rate, $\sigma_{\max}$ is compressive stress, above which restrained growth rate is equal to zero, σ is the average of the principal stresses, σ_{abs} is the absolute of σ and K_1 is the slope of the stress-strain curve.

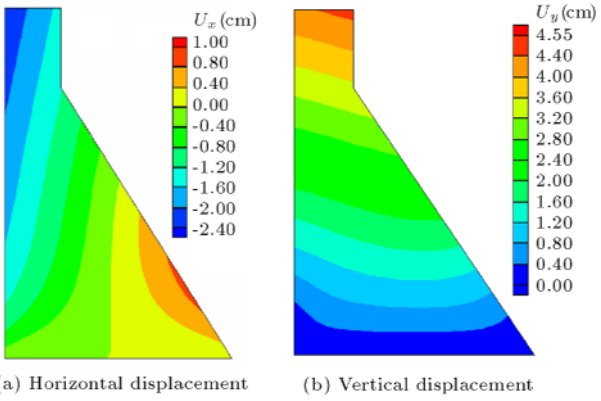

Figure 2. Contours of displacement for isothermal analysis in the first proposed model.

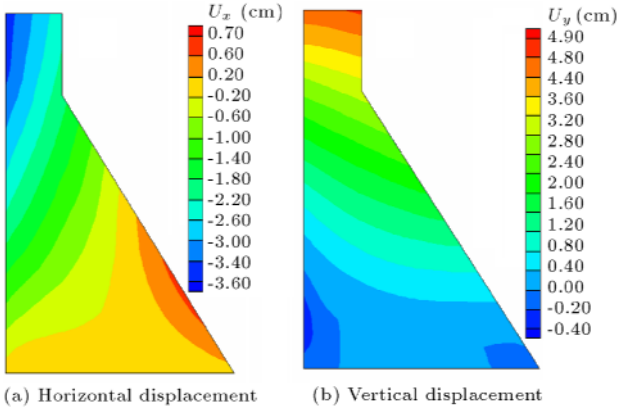

Figure 3. Contours of displacement for nonisothermal analysis in the first proposed model.

Thus, the rate of strain is:

$$\dot{\varepsilon}_{\mathrm{AAR}} = F_\sigma \times F_T \times \dot{\varepsilon}_u. \tag{23}$$

In nonisothermal cases, in the elastic range, the rate of initial strains is equal to:

$$\dot{\varepsilon}_0 = \underbrace{\dot{\varepsilon}_{\mathrm{AAR}}}_{\text{AAR expansion}} + \underbrace{\alpha \dot{T}}_{\text{thermal strain}}. \tag{24}$$

And in isothermal conditions, the thermal effects are relinquished, so:

$$\dot{\varepsilon}_0 = \dot{\varepsilon}_{\mathrm{AAR}}. \tag{25}$$

Degradation of Concrete Properties

In this model, a linear function was used to modify the Young's modulus of elasticity and the compressive strength of the concrete as follows:

$$E = E_0(1 \quad K_2 t), \tag{26}$$

$$f_C = f_{C0}(1 \quad K_3 t). \tag{27}$$

K_2 and K_3 are material constants and t is time. K_2 and K_3 were chosen in a way that E and f_c reach 80 percent of the initial values after 25 years of continuous reaction.

Model Parameters

The numerical simulation was performed using parameters of the model as $\sigma_L = 0.3$ MPa, $\sigma_{\max} = 8$ MPa, $K_2 = K_3 = 0.004$ /year and the calibrated free expansion of 350 $\mu\varepsilon$ /year. The duration of the analysis is 50 years, with one month time step.

Results of Isothermal Analysis

Figure 4 shows the contours of horizontal and vertical displacements computed using the second proposed model in the isothermal case. The horizontal displacement of point A is less than the measured one and the vertical displacements of both points are greater than the measured data.

Results of the Nonisothermal Analysis

Figure 5 shows the contours of horizontal and vertical displacements after 25 years of continuous reaction in the nonisothermal case. The horizontal and vertical displacements of point A were computed. The horizontal computed displacement of point A is less than the measured one, while the vertical displacement of point B is greater than the measured one.

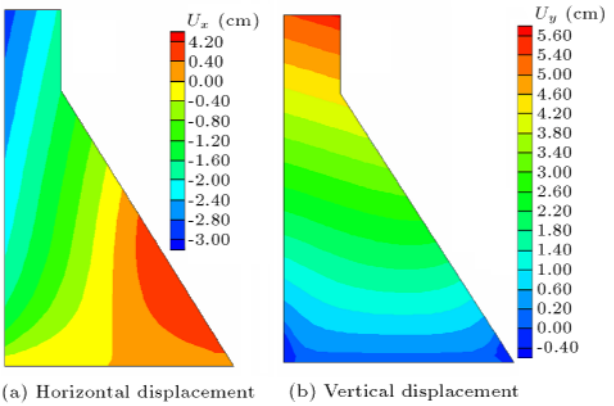

(a) Horizontal displacement (b) Vertical displacement

Figure 4. Contours of displacement for isothermal analysis in the second proposed model.

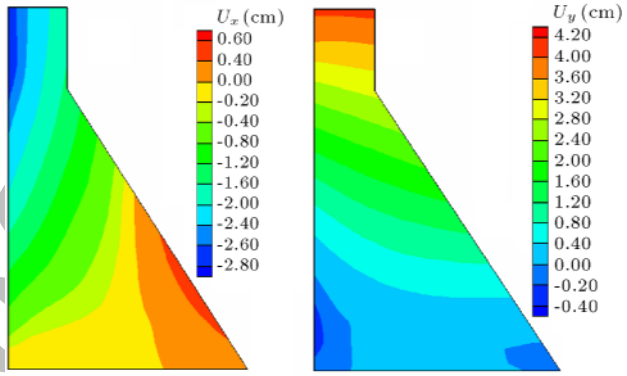

(a) Horizontal displacement (b) Vertical displacement

Figure 5. Contours of displacement for nonisothermal analysis in the second proposed model.

COMPARISON OF THE MODELS

Table 1 shows the comparison of computed displacements of points A and B with the measured displacements. The results of the first proposed model, in the nonisothermal case, are in close agreement with the measured values.

Figures 6 and 7 compare the horizontal and vertical displacement histories of point A, obtained from two models in isothermal and nonisothermal analyses. In the nonisothermal cases, oscillator histories are due to the effect of thermal expansion. During cold weather, the reaction stops, because of the low temperatures. The thermal effects cause the dam to deflect toward downstream. At the beginning of the warm weather, both thermal and AAR strains cause the dam to deflect toward upstream and make an oscillation form in the displacement histories.

To investigate a real dam, using the described models, the constants appearing in F_T and $F_\sigma(\varepsilon, A_3, T_0, A_2)$ are selected, based on experimental results. The remaining material parameters (A_1, B_1 and B_2) are chosen on a rather intuitive basis. Then,

Table 1. Comparison of the results obtained by the proposed models and measured displacement.

Point	Vertical Displacement (cm)					Horizontal Displacement (cm)				
	First Model		Second Model		Measured Values	First Model		Second Model		Measured Values
	Isothermal	Nonisothermal	Isothermal	Nonisothermal		Isothermal	Nonisothermal	Isothermal	Nonisothermal	
A	-1.48	-2.34	-1.93	-1.69	-3.22	4.54	4.87	5.65	4.16	4.88
B	-2.36	-3.64	-3.02	-2.77	-	4.32	4.64	5.37	4.12	3.31

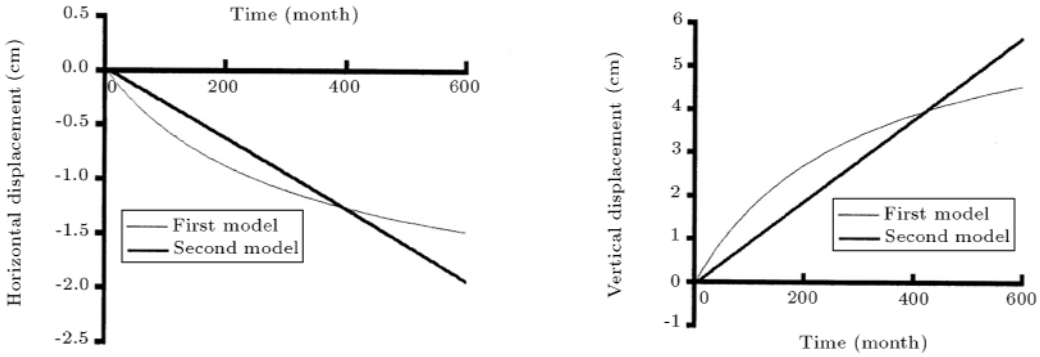

Figure 6. Comparison of isothermal analysis results for point A (at dam crest).

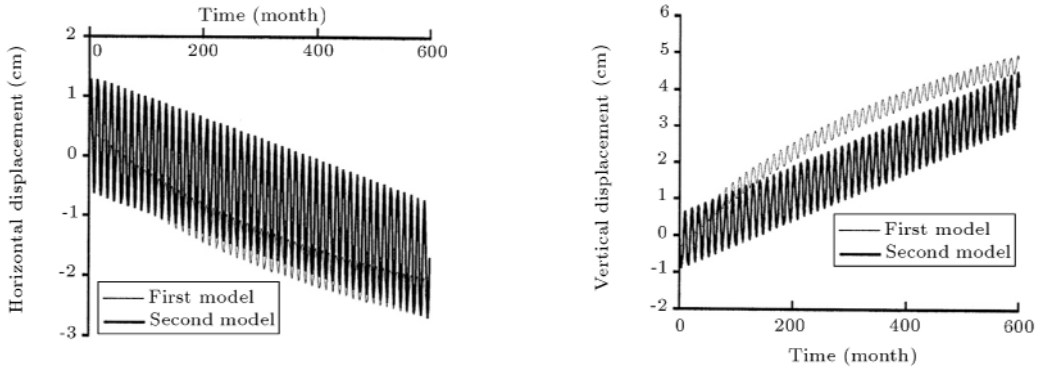

Figure 7. Comparison of nonisothermal analysis results for point A (at dam crest).

the analysis will be carried out using implemented computer subroutines to assess the short and long term effects of AAR. If the AAR caused expansion is relatively high, proper predictions will be necessary.

CONCLUSIONS

In this paper, two models were proposed for modeling the effects of the AAR. They incorporate the effect of AAR expansion coupled with degradation of concrete properties. The main features for initiation and continuation of the reaction in the models are the inclusion of temperature, humidity and applied stresses on the model. The results of the analysis demonstrate the importance of the AAR in concrete dams. High stresses and large deflections occur in the dam during the reaction. Because of the stress dependency of the reaction, vertical displacements are smaller than horizontal displacements.

REFERENCES

1. Charlwood, R.G., Steele, R.R., Solymar, Z.V. and Curtis, D.D. "A review of Alkali aggregate reactions in hydroelectric plants and dams", *Int. Conf. on Alkali-Aggregate Reactions in Hydro-Electric Plants and Dams*, New Brunswick, Canada (Sept. 1992).
2. Leger, P., Cote, P. and Tinawi, R. "Finite element analysis of concrete swelling due to alkali-aggregate reactions in dams", *Computers & Structures*, **60**(4), pp 601-11 (1996).
3. Copra, B. and Bournazel, J.P. "Modelling of induced

mechanical effects of alkali-aggregate reaction", *Cement and Concrete Research*, **28**(2), pp 251-60 (1998).

4. Huang, M., Pietruszczak, S. "Modelling of thermo-mechanical effects of alkali-silica reaction", *Journal of Engrg. Mechanics*, **125**(4), pp 476-85 (April 1999).
5. Bournazel, J.P., Capra, B., Mebarki, A. and Sellier, A. "Alkali-aggregate reaction-a probabilistic description of induced mechanical effects", *Int. Conf. of Computational Modeling of Concrete Structures*, **1**, De Borst. Ed., Mang, Bicanic, Euroc, pp 491-500 (1994).
6. Pleau, R., Berube, M.A., Pigeon, M., Fournier, B. and Raphael, S. "Mechanical behaviour of concrete affected by ASR", *Proc., 8th Int. Conf. on Alkali-Aggregate Reaction*, pp 721-6 (1989).
7. Gocevski, V. and Pietruszczak, S. "On rehabilitation of hydraulic structures subjected to alkali-aggregate reaction", *Numerical Models in Geomechanics-NUMOG VII*, Pande, Pietruszczak & Schweiger, Rotterdam, Balkema, pp 589-94 (1999).
8. Leger, P., Venturelli, J. and Bhattacharjee, S.S. "Seasonal temperature and stress distributions in concrete gravity dams, Part 1: Modelling; Part 2: Behaviour." *Can. J. Civ. Engrg.*, Ottawa, pp 999-1029 (1993).
9. Hobbs, D.W., *Alkali-Silica Reaction in Concrete.*, London (1988).
10. Magni, E.R., Rogers, C.A. and Grattan-Bellew, P.E. "The influence of the alkali-silica reaction on structures in the vicinity of Sudbury", *Ontario. Proc., 7th Int. Conf. on Alkali-Aggregate Reaction in Concrete*, pp 17-21 (1986).

Scientia Iranica, Vol. 15, No. 1, pp 8 15

SCIENTIA IRANICA

Interpretation of Tensile Softening in Concrete, Using Fractal Geometry

H. Khezrzadeh[1] **and M. Mofid**[*]

Concrete is a heterogeneous material with a wide variety of usage in structural design. Concrete under tension exhibits strain softening, i.e., a negative slope in the stress deformation diagrams. Different softening curves have been proposed in the literature to interpret this phenomenon. In current research, a new softening curve for concrete has been proposed by using the newly introduced concept of fractal geometry. This new softening curve is denominated a 'Quasi-fractal' softening curve and consists of two parts, a linear portion at the beginning and an exponential portion in the rest of the curve. A comparison of a "Quasi-fractal" softening curve with a set of proposed experimental softening curves has been performed, which reveals good agreement.

INTRODUCTION

Since its first presentation by Mandelbrot [1], fractal geometry has found many applications in science and technology. The main merit of this new mathematical tool is in its ability to model natural irregularities. Owing to this, fractal geometry has found many applications, such as in electromagnetic, biology, fluid mechanics and many branches of solid and fracture mechanics.

The first step in using this new concept in fracture mechanics is the verification of the fact that fracture surfaces have fractal patterns. Several experiments and theory outcomes confirm that fracture surfaces in many engineering materials are fractal. The first investigation into this field concerned the fractal character of fracture surfaces in metals, which was carried out by Mandelbrot et al. [2]. Subsequently, some efforts were made to characterize the fracture surfaces of concrete. Among those researchers, one should mention Winslow [3], Saouma et al. [4], Brandt and Prokopski [5], Saouma and Barton [6], Carpinteri et al. [7] and Issa et al. [8]. In addition to the aforementioned experimental evidence of the hypothesis of the fractality of the fracture surfaces of concrete, theoretical proof also exists, such as in Carpinteri et al. [9].

Fracture in heterogeneous materials, e.g. concrete, is one of the most active branches in fracture mechanics. Resulting from inhomogeneities inside the structure of such materials, one of the best ways to analyze the behavior of these kinds of material is by the use of fractal geometry.

It is known that classes of material, such as concrete, rock, brick and ceramics, exhibit what is termed 'strain-softening' behavior. Thus, in a direct tensile test, there is a linear stress-strain relationship until, approximately, the ultimate strength, σ_u, is reached and further straining beyond this point results in stress relaxation, which depends on the strain-softening characteristics of the material. The ultimate behavior of such materials is characterized by the localization of a non-linear zone within a narrow band of the material, while the rest of the material outside this softening zone retains its linear behavior. In the cohesive model, this band is treated as the softening zone, where the material, though cracked, can still transfer stress. The tensile stress, σ, in the softening zone is described as the decreasing function of the relative displacement, w, of the opposite surfaces of the cohesive crack. The process zone starts forming after the tensile stress reaches its ultimate value, σ_u. The point where the displacement, w, reaches its critical value, w_c, beyond which no stress can be transferred, is called the real crack tip, while the point along the cohesive crack, at which the stress reaches σ_u, is called the cohesive crack tip. There are no stress singularities present in this model.

The "cohesive crack model" was described by Barenblatt [10,11] and Dugdale [12]. Many researchers have used cohesive cracks to describe the near-tip non-

1. *Department of Civil Engineering, Sharif University of Technology, Tehran, I.R. Iran.*
*. *Corresponding Author, Department of Civil Engineering, Sharif University of Technology, Tehran, I.R. Iran.*